

**Brightening dark excitons and trions in systems with a  
Mexican-hat energy dispersion: example of InSe**

Lewis J. Burke,<sup>\*</sup> Mark T. Greenaway,<sup>†</sup> and Joseph J. Betouras<sup>‡</sup>

*Department of Physics and Centre for the Science of Materials,*

*Loughborough University, LE11 3TU, United Kingdom*

(Dated: February 11, 2025)

arXiv:2502.06473v1 [cond-mat.mes-hall] 10 Feb 2025

## Abstract

We investigate the properties of momentum-dark excitons and trions formed in two-dimensional (2D) materials that exhibit an inverted Mexican-hat-shaped dispersion relation, taking monolayer InSe as an example. We employ variational techniques to obtain the momentum-dark and bright ground-states (non-zero and zero quasiparticle momenta, respectively). These states are of particular interest due to their peaks in the quasiparticle density of states, the largest contribution comes from the momentum-dark ground state due to the presence of a van Hove singularity (VHS). These momentum-dark systems require a physical process to provide the necessary momentum to become bright. We study the brightening of this state due to coupling with phonons and compute the resulting photoluminescence spectrum. This work opens new avenues of research, such as exploiting dark excitons in solar cells and other semiconductor-based optoelectronic devices.

Two-dimensional (2D) van der Waals (vdW) materials offer promising prospects for both fundamental physics research and a wide range of technological applications [1]. 2D vdW semiconductors with finite bandgaps [2, 3], are particularly promising materials for nanoelectronics and photonics [4, 5]. As a result, understanding these materials' excitonic and optical properties is important as they present new paradigms compared to traditional semiconductors. For example, their weak dielectric screening and strong geometrical confinement give rise to strong Coulomb interaction effects, resulting in rich many-particle phenomena, such as forming a variety of different excitons [6, 7], which includes bright and dark excitons.

There are two types of dark excitons (excitons that cannot emit light efficiently due to selection rules): spin-dark, [8–10] when the electron and hole have opposite spin [11], and momentum-dark [10, 12]. A momentum-dark (or momentum-forbidden) exciton is one in which the electron and hole are at different points in momentum-space, such as different valleys in transition metal dichalcogenides (TMDs)[13]. Here, a photon can provide enough energy to activate a dark state, but it cannot provide the momentum to create a bright excitonic state. The dark state energy is thus often lower than their bright counterparts [14]. Momentum-dark excitons can be observed experimentally if they couple to phonons [15, 16] (and spin-dark excitons if they couple with an in-plane magnetic field [17]).

Other interesting many-body excitonic states in vdW materials include interlayer excitons

---

\* L.J.Burke@lboro.ac.uk

† M.T.Greenaway@lboro.ac.uk

‡ J.Betouras@lboro.ac.uk

[18, 19] - moiré excitons [20, 21], biexcitons [22] and trions [23]. A trion is a direct extension of an exciton. This is through adding an extra electron or hole to the system (commonly via electron or hole doping), and consequently, they are negatively or positively charged. This is described as a three-particle complex of a charged exciton [23, 24], which can be classified as either a singlet or a triplet [25], depending on the spin-state of the extra particle. If the pair of spins of the electron (negative trion) and the hole (positive trion) are aligned, we have a triplet state and anti-aligned we have a singlet state.

There are other descriptions for a trion which describe it with a four-body Schrödinger equation, which includes a conduction band hole in the case of an electron-doped system [26, 27]. Dark excitons and trions have longer lifetimes than bright states, with lifetimes roughly of the order of nanoseconds [28, 29]. Therefore, they have potential applications for semiconductor-based optoelectronic devices and solar cell devices for both bright and dark states [30].

Experimentally, trion formation in doped systems is realised by electrostatic gating, which can be tuned to allow the formation of positive or negative trions. The resulting exciton and trion photoluminescence (PL) peaks can be measured and analysed [31, 32]. Much of the experimental work has been on TMDs, such as  $\text{WSe}_2$  [32]. Here, the 2D material is encapsulated by hexagonal boron nitride (hBN) and electrostatic gating is used to control charge and form new bound states. In order to link this experimental work with the theoretical calculations and to study the measured PL and signatures of the trions, recently, a generalised PL formula has been developed that captures both bright and dark trion states via the inclusion of direct and in-direct (phonon-assisted recombination) [33], extending previous work on the excitonic states [10, 11, 13].

InSe is a 2D semiconductor comprising 4-atom thick monolayers, of covalently bonded Se-In-In-Se atoms, with vdW interlayer bonding. It has shown great potential due to its promising performance in optoelectronic devices and potential for strain engineering and nonlinear optics [34–38]. An unusual feature of monolayer InSe is the dispersion relation of its valence band, which exhibits a band inversion around the  $\Gamma$ -point known as a Mexican-hat-shaped dispersion [39]. This form of dispersion relation has been shown to give rise to very interesting properties under certain conditions [40, 41]. In addition, there is a growing interest in systems, such as monolayer InSe, that host Van Hove singularities (VHS) and flattened bands, due to pronounced interaction effects [42–44]. These features make InSe a

paradigmatic material for experimental and theoretical investigations [28, 39, 45, 46]. To ensure high sample quality, InSe is often encapsulated with hBN, which we will take into account in this work. We use a variational approach, based on the 1s hydrogen ground-state wave function, to analyse in detail the exciton physics due to the inverted Mexican-hat present in monolayer InSe. We then investigate the properties of positive and negative trions obtained via hole and electron doping and compare the two and three-quasiparticle ground-state dispersions. The lowest-energy states are momentum-dark. Thus, we also investigate a brightening mechanism via coupling to a phonon to create a virtual bright state to explore the PL spectra.

Our work compares these excitonic and trionic systems. We find strong peaks in the density of states (DOS) of the exciton and trion systems. The peaks at the quasiparticle band minimum correspond to the momentum-dark state, suggesting that the dark states could have a large effect on the optical properties of the system. This is a direct result of the Mexican-hat-shaped valence band dispersion. Our work further reveals that for the electron-doped system, the negatively charged trion at low temperatures dominates the PL intensity. However, as temperature increases, the excitonic intensity becomes more substantial. In the hole-doped system, which can lead to the formation of a positively charged trion, the momentum bright and dark trion's are weakly bound and are comparatively an energetically unfavourable ground-state quasiparticle state of the system compared to that of the exciton. Our work is easily extended to other 2D materials with Mexican-hat dispersions, such as GaSe.

## I. RESULTS AND DISCUSSION

### A. Monolayer InSe

InSe is an III-VI chalcogenide (metal-group III atom and group VI-chalcogenide), with a hexagonal structure with unit vectors  $\mathbf{a}_1 = (a/2, \sqrt{3}a/2)$  and  $\mathbf{a}_2 = (a/2, -\sqrt{3}a/2)$ , where  $a = 3.95 \text{ \AA}$  is the lattice constant. The reciprocal primitive lattice vector vectors are  $\mathbf{b}_1 = (2\pi/a, 2\pi/\sqrt{3}a)$  and  $\mathbf{b}_2 = (2\pi/a, -2\pi/\sqrt{3}a)$ . The high symmetry points  $\Gamma$ ,  $K$ ,  $M$  of the hexagonal Brillouin zone (BZ) are:  $\Gamma = (0, 0)$ ,  $K = (4\pi/3a, 0)$  and  $M = (\pi/a, -\pi/\sqrt{3}a)$ .

In Fig. 1a, we show the band structure and DOS for monolayer InSe obtained using

Density Functional Theory (DFT) (see Sec. IID). It reveals an inverted Mexican-hat shape is present in the top-most valence band at which a VHS is present at the brim of the hat, whereas the conduction band can be modelled by a parabolic expression (see Fig. 1b).

DFT underestimates the size of the bandgap. However, in both excitonic and trionic systems, under the condition of the bandgap being much greater than the binding energy (which implies that we can ignore the overlaps of the electronic states), the binding energy is independent of the bandgap. In Fig. 1b, near the  $\Gamma$ -point, the highest valence band and

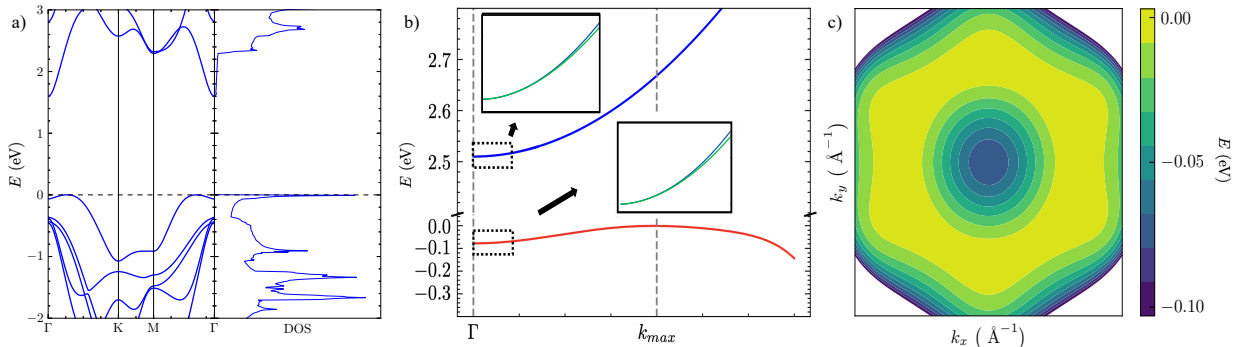


FIG. 1. a) (left) Monolayer InSe band structure determined by DFT calculations (see Sec. IID)  $E = 0$  at valence band maximum, (right) density of states. b) Conduction and valence band determined by the polynomial expression in Eqs. (1-2) c) Colour map of the top-most valence band

lowest conduction band are modelled by the following polynomial expressions [47]:

$$\begin{aligned}
 E_c(\mathbf{k}) &= \frac{|\mathbf{k}|^2}{2m_e^*} + E_c^{SO}(\mathbf{k}) \\
 E_v(\mathbf{k}) &= E_0 + E_1|\mathbf{k}|^2 + E_2|\mathbf{k}|^4 + E_3|\mathbf{k}|^6 \\
 &\quad + E_4|\mathbf{k}|^6 \cos(6\varphi) + E_5|\mathbf{k}|^8 + E_v^{SO}(\mathbf{k})
 \end{aligned}
 \tag{1}$$

The parameters are defined in Table I.

DFT calculations show that spin-orbit coupling (SOC)-induced splitting is small, but for completeness and the trion calculations, we include these contributions in Eq. (1). The terms for the lowest conduction band and highest valence band for the monolayer system, close to the  $\Gamma$ -point are:

$$\begin{aligned}
 E_c^{SO}(\mathbf{k}) &= \gamma_c s_z |\mathbf{k}|^3 \cos(3\varphi) \\
 E_v^{SO}(\mathbf{k}) &= \gamma_v s_z |\mathbf{k}|^3 \cos(3\varphi)
 \end{aligned}
 \tag{2}$$

$E_0$	-0.078	eV
$E_1$	2.915	eV $\text{\AA}^2$
$E_2$	-38.057	eV $\text{\AA}^4$
$E_3$	205.551	eV $\text{\AA}^6$
$E_4$	3.050	eV $\text{\AA}^6$
$E_5$	-450.034	eV $\text{\AA}^8$
$m_e^*$	0.188	$m_e$

TABLE I. Parameters from [47]

where  $\gamma_c = 1.49 \text{ eV \AA}^3$  and  $\gamma_v = 3.11 \text{ eV \AA}^3$  [47] and  $s_z = \pm\frac{1}{2}$ . This ignores the direct effects of the interaction of the SOC bands, which will be discussed later in this section.

## B. Excitons

To obtain the ground-state exciton energy,  $E_{ex}(\mathbf{k})$ , in which the electron and hole are at the extrema of the uppermost valence band and lowest conduction band (both of the same spin), we consider the eigenvalue Bethe-Salpeter approach, described in Sec. II A. The valence band maximum (VBM), in monolayer InSe, occurs at  $\mathbf{k} = \mathbf{k}_{max} \approx (0.28, 0) \text{ \AA}^{-1}$ , which contributes to the degree of how "dark" the system is.

The binding energy is determined from the calculated exciton energy:

$$E_{ex}^b(\mathbf{Q}_{min}) = E_{ex}(\mathbf{Q}_{min}) - E_g \quad (3)$$

where  $E_g$  is the the bandgap energy and  $\mathbf{Q}_{min}$  is the wave vector of the lowest exciton state.  $\mathbf{Q}_{min} \neq \mathbf{0}$  implies we have a non-zero momentum lowest energy excitonic state. The energy difference between the  $\mathbf{Q} = \mathbf{Q}_{min}$  and  $\mathbf{Q} = \mathbf{0}$  states gives us the activation energy required to brighten the dark state [46]

$$E_{ex}^{act} = E_{ex}(\mathbf{Q}_{min}) - E_{ex}(\mathbf{0}). \quad (4)$$

The activation energy thus provides a measure of how distinguishable the bright and dark states would be in an experiment. The calculated excitonic binding energy dispersions are shown in Fig. 2, where  $\mathbf{Q}$  is the exciton momenta. We find the exciton preserves the hexagonal symmetry of the valence band ( $E_4 k^6 \cos(6\varphi)$ ) and also exhibits a Mexican hat

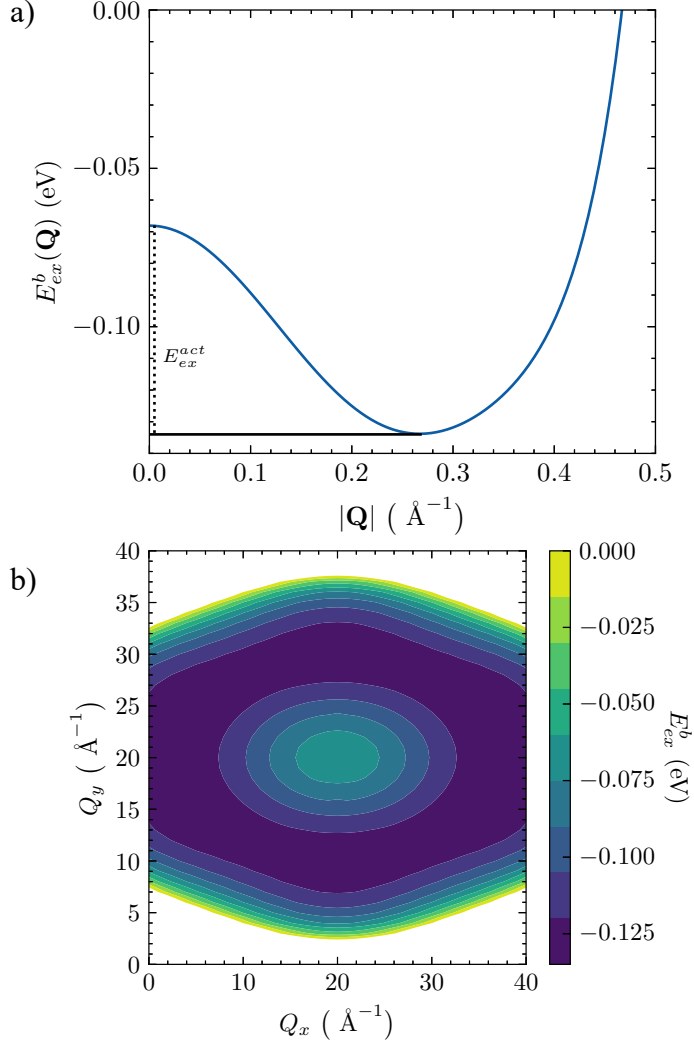


FIG. 2. a) Exciton dispersion,  $E_{ex}(\mathbf{Q})$ , in the  $\Gamma \rightarrow K$  direction. The momentum-dark exciton state is at  $\mathbf{Q}_{min}$ . b) Colour map of the exciton dispersion, which reveals the Mexican hat nature over the reduced BZ and the preservation of the hexagonal symmetry.

shaped-dispersion. This momentum-dark exciton has a ground-state binding energy and activation energy of:

$$E_{ex}^b(\mathbf{Q}_{min}) = -135 \text{ meV}, \quad E_{ex}^{act} = 65 \text{ meV}. \quad (5)$$

The variational calculations provide the value for  $\beta$  at the finite momentum-state,  $\mathbf{Q}_{min}$ , from which we obtain an exciton radius of:

$$r_{ex} = \frac{1}{\beta} \approx 17 \text{ \AA}. \quad (6)$$

we find,  $\lambda = 1.03 \approx 1$ , confirming that the state is isotropic. As this model is appropriate for a Wannier-Mott type exciton and has a relatively large radius, it can be concluded that this is a relatively weakly bound exciton.

### C. Trion

We subsequently consider the energy of the trion quasiparticle following the method described in Sec. II B. Both positive and negative trions are considered, by adding either an extra hole or an electron to the exciton. We introduce these particles so that they have opposite spin to the ones present in the exciton system, meaning the electron and hole spin-states in their respective trions are anti-aligned, leading to the description of singlet trions (see inset of Fig. 1b), which highlights the SOC splitting of the conduction and valence band. This system can be obtained via electron or hole doping (e.g. by the application of gate voltages [48, 49]) that creates an electron of opposite spin in the bottom-most spin-split conduction band or the annihilation of another electron in the spin-split valence band. In Sec. II B, we describe the method to determine the trion energy for the positively and negatively charged trion from which we determine the total binding energy of the three-particle systems,

$$\begin{aligned} E_{tr,-}^{b,tot}(\mathbf{Q}) &= E_{tr,-}(\mathbf{Q}) - 2E_g \\ E_{tr,+}^{b,tot}(\mathbf{Q}) &= E_{tr,+}(\mathbf{Q}) - E_g \end{aligned} \quad (7)$$

from this, we can obtain the trion's binding energy measured with respect to the exciton's binding energy, this is given as [26, 50]:

$$E_{tr,\pm}^b(\mathbf{Q}) = E_{tr,\pm}^{b,tot}(\mathbf{Q}) - E_{ex}^b(\mathbf{Q}) \quad (8)$$

$E_{tr}^b(\mathbf{Q})$  is the energy required for the extra particle to bind to the exciton to form the trion. In Fig. 3b, we show the total three-particle binding energies to compare to the excitonic state, the momentum of the minimised state is indicated by  $\mathbf{Q}_{min}$ . For the momentum-dark trion at  $\mathbf{Q} = \mathbf{Q}_{min}$  we obtain:

$$\begin{aligned} E_{tr,+}^b(\mathbf{Q}_{min}) &= 65 \text{ meV}, & E_{tr,+}^{act} &= 65 \text{ meV} \\ E_{tr,-}^b(\mathbf{Q}_{min}) &= -10 \text{ meV}, & E_{tr,-}^{act} &= 65 \text{ meV} \end{aligned} \quad (9)$$



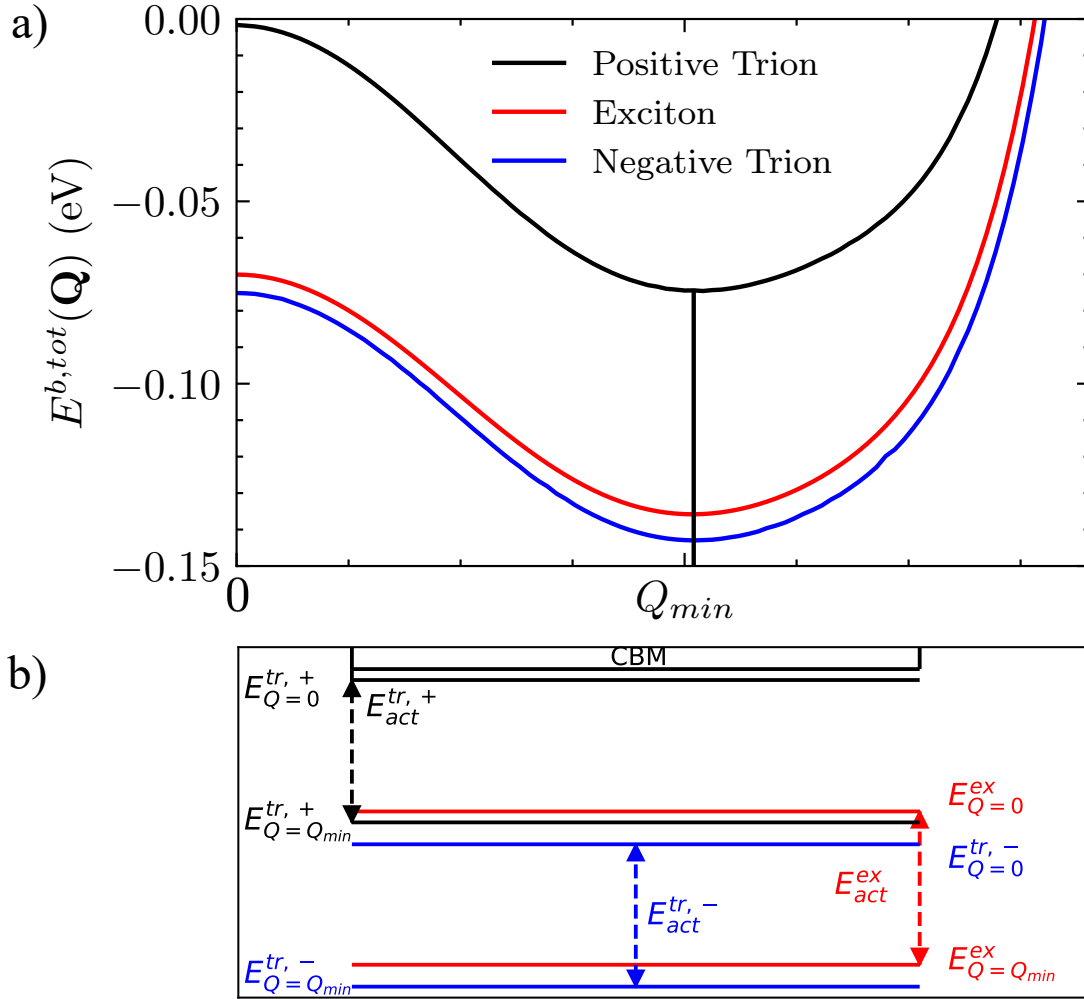


FIG. 3. a) Total three-particle (trion) and two-particle (exciton) binding energies with  $Q_{min}$  indicated. b) Indication of the bright and dark states for each bound state system with the activation energies indicated with respect to the conduction band minimum (CBM).

Fig. 3a shows that the three-particle negative trion energy system is more strongly bound than both the exciton and the positive trion systems. The binding energy of the hole to form the positive trion is positive, so it reduces the total binding energy of the three-particle system, this is due to the strong hole-hole interaction at the VHS of the valence band. This result shows that for the hole-doped system, the favourable configuration of the electron and holes is the formation of the exciton-bound state with the addition of a free hole rather than the positively charged trion. This is unlike the electron-doped system which has a negative trion binding energy which leads to a more energetically favourable configuration for the

trion system.

The trion has two length scales given by, radius,  $r_1^{tr}$  and  $r_2^{tr}$ , which are determined by the variational parameters as:

$$r_1^{tr} = \frac{1}{\alpha} \approx 15 \text{ \AA}, \quad r_2^{tr} = \frac{1}{\gamma} \approx 50 \text{ \AA}. \quad (10)$$

The trion system is characterised by two different "radii" resulting from the superposition of states in the variational wave function. The values of  $r_{1,2}^{tr}$  are effectively the values of the radius of each electron and hole pair comprising the trion. These two radii imply that in the case of the negative (positive) trion, one electron (hole) sits close to the exciton radius, while the other sits further away, which minimises the like-charge repulsive interaction, this is consistent with the behaviour obtained in Ref. [51].

#### D. Photoluminescence (PL)

Using these excitonic and trionic structures, we study how the bright and dark states (visualised in Fig. 3b)) impact the PL spectrum. The recombination of the electron-hole bound system of the bright state allows the direct emission of a luminescence photon (direct PL). Dark states require phonon coupling to transfer momentum to create a virtual bright state, which leads to indirect PL, see Fig. 4. To account for the phonon coupling, we consider a polaron picture, which can be reduced to a simple phonon scattering process to generate a virtual-bright state. In monolayer InSe, electron-phonon scattering is dominated by longitudinal optical (LO) phonons. Whereas for hole-phonon scattering, the longitudinal acoustic (LA) phonons provide the largest contribution [28, 52]. In this work, we consider a single LA phonon that scatters the hole at the valence band maximum, which is at the brim of the Mexican-hat [52]. Given the stronger hole scattering we assume that the emission of a LA phonon with a momentum equal to  $\mathbf{k}_{max}$  and energy  $E_{ph}(\mathbf{k}_{max})$  (see Fig. 5) can lead to the brightening of the dark state [28]. This point is described in detail in Sec. II C. Effectively the phonon coupling increases the ground-state energy of the dark state which stems from the non-interacting part of the BSE equation. The expression for the virtual bright state is given in Eq. (45) of Sec II C. The result for the exciton virtual-bright state energy due to this change is:

$$E_{ex,ph}^b(\mathbf{Q} = \mathbf{0}) = E_{ex}^b(\mathbf{Q} = \mathbf{Q}_{min}) + E_{ph}(\mathbf{k}_{max}) \quad (11)$$

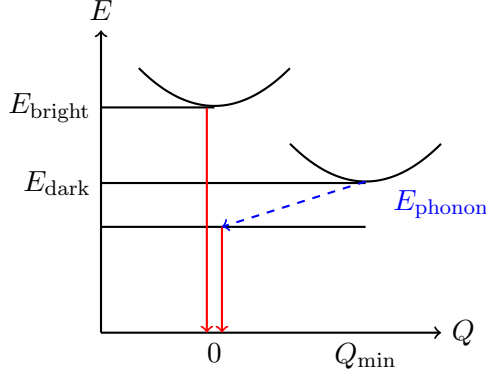


FIG. 4. Bright ( $Q = 0$ ) and Dark ( $Q = Q_{min}$ ) excitonic states indicated by parabolic dispersion, showing a phonon-assisted transition through emission to a lower virtual bright state.

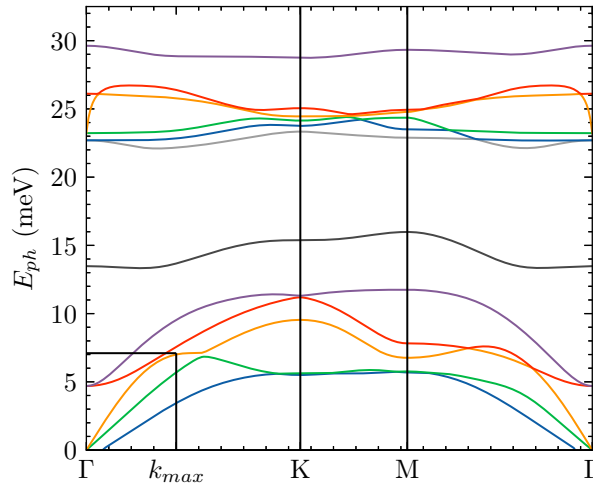


FIG. 5. Monolayer InSe phonon dispersion relation determined using DFT.

Similarly, for the trion, we require the electron and hole pair of the same spin to be at the same point in momentum-space and for both the negative and positive trions thus, the continuation is identical to that of the exciton:

$$E_{tr,ph}^{b,\pm}(Q = 0) = E_{tr,\pm}^b(Q = Q_{min}) + E_{ph}(k_{max}). \quad (12)$$

These states help us populate Fig. 6, which is a schematic indicating the bright states and the virtual bright states resulting from the phonon transition.

In the PL spectrum we include the contributions of direct and indirect PL ( $Q = 0$  and  $Q = Q_{min}$ ) contributions for the excitonic [53, 54] and trionic states [33]. However, as previously mentioned, we ignore the unbound bright positive trion state in the hole-doped

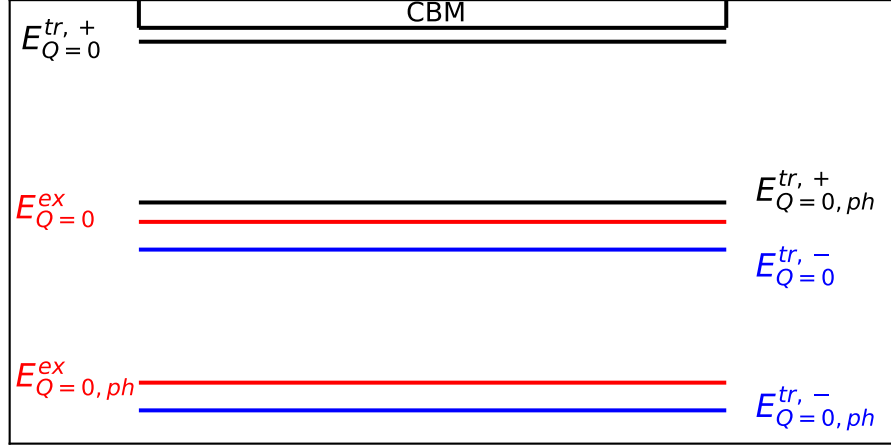


FIG. 6. Exciton and trion energies below the conduction band minimum (CBM), including bright state ( $E_{\mathbf{Q}=\mathbf{0}}$ ) and virtual bright state ( $E_{\mathbf{Q}=\mathbf{0},ph}$ ). These energies correspond to peaks in the photoluminescence spectrum; the black/blue lines correspond to the positive/negative trion, and the red lines correspond to the exciton.

system. We consider these states for the PL calculation due to their large density of states, see Fig. 7, where we show the exciton and trion density of states calculated using:

$$g(E) = \sum_{\mathbf{Q}} \delta(E - E^{b,tot}(\mathbf{Q})) \approx \frac{1}{\sqrt{2\pi}\sigma} \sum_{\mathbf{Q}} \exp\left(\frac{-(E - E^{b,tot}(\mathbf{Q}))^2}{2\sigma^2}\right). \quad (13)$$

We obtain two distinct peaks corresponding to the dark and bright states. The lowest energy dark state has a more pronounced peak for each quasiparticle density of states. This is due to the VHS present in their respective energy dispersion. The result of this is that the PL spectrum will be dominated by these states due to their large DOS contribution. We determine the excitonic contribution to the PL spectrum due to the bright (b) and dark (d) (virtual-bright) states using the following expressions [54]:

$$PL^b(\omega) \propto \frac{|M_{\mathbf{k}}|^2 \gamma_{rad} N_{\mathbf{Q}=\mathbf{0}}}{(E_{ex}(\mathbf{Q}=\mathbf{0}) - \omega)^2 + (\gamma_{rad} + \Gamma_{phonon})^2} \quad (14)$$

$$PL^d(\omega) \propto \frac{|M_{\mathbf{k}}|^2}{(E_{ex}(\mathbf{Q}=\mathbf{0}) - \omega)^2 + (\gamma_{rad} + \Gamma_{phonon})^2} \times \frac{|D_{\mathbf{Q}}|^2 N_{\mathbf{Q}=\mathbf{Q}_{min}} \eta_{\mathbf{Q}} \Gamma_{phonon}}{(E_{ex,ph}(\mathbf{Q}=\mathbf{0}) - \omega)^2 + (\Gamma_{phonon})^2} \quad (15)$$

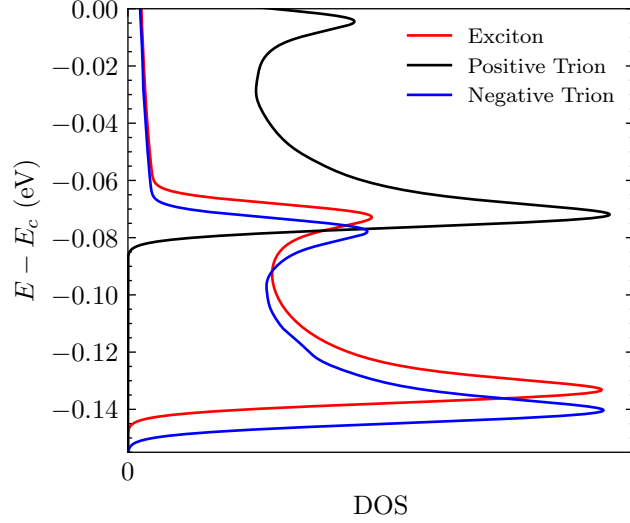


FIG. 7. Exciton and trion DOS (using Eq. (13) along with results indicated in Fig. 3). This highlights two pronounced peaks for each quasiparticle state, the larger peak corresponds to the dark state at which a VHS is present, while the other peak corresponds to the bright state.

where  $M_{\mathbf{k}}$  is the matrix element of the exciton-photon interaction,  $N_{\mathbf{Q}}$  and  $\eta_{\mathbf{Q}}$  are the exciton and phonon occupation factors,  $D_{\mathbf{Q}}$  represents the phonon-exciton interaction matrix and  $\gamma_{rad}, \Gamma_{phonon}$  are the radiative and phonon-assisted dephasing of the relevant excitonic states.

We consider circularly polarised light  $\sigma^-$ , so that the exciton-photon matrix element is:

$$|M_{\mathbf{k}}|^2 = |P_{cv}(\mathbf{k}) \cdot e_{\sigma^-}|^2 \quad (16)$$

where  $P_{cv}(\mathbf{k})$  is the interband matrix element which is calculated using the tight-binding model of Ref [47] so that:

$$\begin{aligned} P_{cv}(\mathbf{k}) &= \langle c | \nabla_{\mathbf{k}} H | v \rangle \\ &= \sum_{o, o'} C_{c, \mathbf{k}}^\dagger(o) C_{v, \mathbf{k}}(o') \nabla_{\mathbf{k}} \langle o | H(\mathbf{k}) | o' \rangle \end{aligned} \quad (17)$$

where the summation is over the orbitals involved in the tight-binding model. The full expression for the PL exciton spectrum can be written as:

$$\begin{aligned} PL^{ex}(\omega) &= 2 \left( \frac{|P_{cv}(\mathbf{k}) \cdot e_{\sigma^-}|^2}{(E_{ex}(\mathbf{Q} = \mathbf{0}) - \omega)^2 + (\gamma_{rad} + \Gamma_{phonon})^2} \right) \\ &\times \left[ N_{\mathbf{Q}=\mathbf{0}} \gamma_{rad} + \frac{|D_{\mathbf{Q}}|^2 N_{\mathbf{Q}=\mathbf{Q}_{min}} \eta_{\mathbf{Q}} \Gamma_{phonon}}{(E_{ex,ph}(\mathbf{Q} = \mathbf{0}) - \omega)^2 + (\Gamma_{phonon})^2} \right] \end{aligned} \quad (18)$$

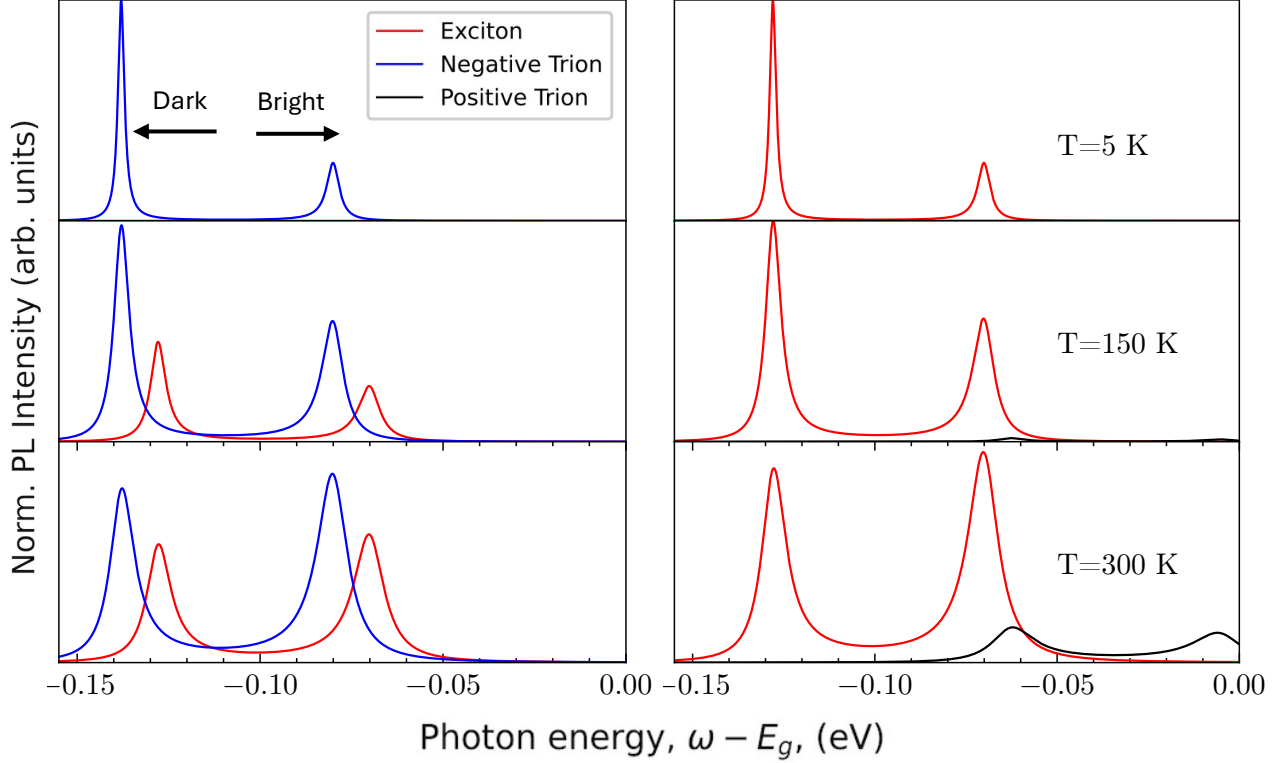


FIG. 8. PL spectrum for the excitonic and trionic contributions. (Left column) compares the exciton (red) and negative trion (blue) in the electron-doped system. (Right column) compares the exciton (red) and positive trion (black) in the hole-doped system. Each row shows how the spectra evolves through temperatures  $T = 5, 150$  and  $300$  K. The peak positions slowly change with temperature; this is purely the effect of the dark states. The peaks on the LHS of each pair correspond to the dark (virtual bright) state, and the RHS peak corresponds to the direct PL peak.

where the peaks of the spectrum correspond to the photon energy ( $\omega$ ), which matches the bright or virtual-bright state excitonic energy. The trion PL spectrum contribution for both systems is given by [33]:

$$\begin{aligned}
& PL^{tr,\pm}(\omega) \\
&= 2 \left( \frac{|M'_{\mathbf{k}}|^2}{(E_{tr}^{\pm}(\mathbf{Q} = \mathbf{0}) - E_{\mathbf{k}}^{h/e} - \omega)^2 + (\gamma_{\pm}^{tr,1})^2} \right) \\
&\times \left[ N_{\mathbf{Q}=\mathbf{0}} \gamma^{tr,2} + \frac{N_{\mathbf{Q}=\mathbf{Q}_{min}} |G_{\mathbf{Q}}|^2 \eta_{\mathbf{Q}} \gamma_{\pm}^{tr,3}}{(E_{tr,ph}^{\pm}(\mathbf{Q} = \mathbf{0}) - E_{\mathbf{k}}^{h/e} - \omega)^2 + (\gamma_{\pm}^{tr,3})^2} \right]
\end{aligned} \tag{19}$$

where:

$$\begin{aligned}
\gamma_{\pm}^{tr,1} &= \gamma^{tr+photon} + \gamma_{\pm}^{tr+phonon} \\
\gamma_{\pm}^{tr,2} &= \gamma^{tr+photon} \\
\gamma_{\pm}^{tr,3} &= \gamma_{\pm}^{tr+phonon}
\end{aligned} \tag{20}$$

where we ignore the separate phonon dephasing of the trion due to the electron or hole that remains after the recombination process. Here  $M'_{\mathbf{k}}$  represents the trion-photon matrix element and  $|G_{\mathcal{Q}}|$  represents the trion-phonon interaction matrix. In this case, we assume that the excitonic and trionic phonon couplings and interband transition remain the same. The exciton and trion occupations are approximated via the Boltzmann distribution and the phonon occupation is via the Bose-Einstein distribution [33, 54]. This is paired with the recoil hole or electron,  $E_{\mathbf{k}}^{h/e}$ , [33], which is the energy present to preserve energy and momentum conservation and a result of the recombination process. In this, we use the assumption that all the momenta involved in the recombination process is given to the luminescence photon. Therefore, in these trion systems, we define the recoil energies as the energy of the remaining particle. For the negative trion, the extra electron is situated at the CBM at  $\mathbf{k} = 0$ . Thus the recoil energy is:  $E_{\mathbf{k}}^e = E_c(\mathbf{k} = 0) = E_g$ . For the positive trion, the extra hole is situated at the VBM at  $\mathbf{k} = \mathbf{k}_{max}$ , which is defined at  $E = 0$ . Thus the recoil energy is:  $E_{\mathbf{k}}^h = E_v(\mathbf{k} = \mathbf{k}_{max}) = 0$ .

In Fig. 8, we show the PL intensity spectrum for three different temperatures (5, 150, 300 K) for both electron and hole-doped systems. For the radiative dephasing for the exciton and trion, we use an indicative value of 1 meV, and for the phonon-induced dephasing, we adopt the following temperature dependence [33].

$$\begin{aligned}
\Gamma_{phonon} &= 1 \text{ meV} + (0.01 \text{ meV/K}) T \\
\gamma_{-}^{tr+phonon} &= 1 \text{ meV} + (0.01 \text{ meV/K}) T \\
\gamma_{+}^{tr+phonon} &= 1 \text{ meV} + (0.02 \text{ meV/K}) T
\end{aligned} \tag{21}$$

In the electron-doped system at low temperatures, the negative trion dominates the PL intensity, with the left peak, which corresponds to the dark virtual state, being much more pronounced than the bright peak. This is because the higher energy state has lower occupation, therefore, the recombination process of the trion system is via the dark state and phonon-assisted transitions (as discussed in [53]). With increasing temperature, the bright

peak becomes more pronounced than the dark virtual state peak and the contribution from the exciton also increases. At 300 K the trion and exciton peaks have similar intensities. In an experiment, this may be observed as one single broadened peak as seen for systems which exhibit these quasiparticles [55, 56]. This behaviour can be explained by considering two key points: firstly, the dephasing dependence on temperature is similar for both quasiparticles under the assumption of a dominant LA phonon coupling. Secondly, at low temperatures when  $k_B T$  is less than the binding energy, the thermal energy is not large enough to destroy the trion state, and the trion bound state would be more energetically favourable due to its larger total binding energy. However, as the thermal energy becomes comparable to or greater than the trion's binding energy, there is a dissociation of the free electron and the exciton (which is still formed due to its higher binding energy). Therefore the trion state becomes less favourable and at 150 K ( $\approx 13$  meV), we see a reduction in the relative strength of the trion peak and its contribution to the PL spectrum.

The temperature dependence of the PL in the hole-doped system (and positive trion) is different. We find the PL intensity of the positive trion has a much smaller relative intensity compared to the exciton for all temperatures. This is expected since the exciton is the more energetically favourable quasiparticle state. We note that the positive trion will have a much shorter lifetime in comparison to the dominating exciton peaks and would thus be difficult to observe experimentally.

Temperature also plays a role in the energy difference between peaks in the PL spectrum corresponding to the dark and bright states (related to the activation energy in the quasiparticle energy spectrum). This is due to the change in the luminescence photon energy, which corresponds to the dark-virtual state. As temperature is increased, the phonon-induced dephasing term also increases (see Eq. 21), resulting in a small shift of the dark peak so that it moves closer to the bright state peak. Eventually, the two peaks are no longer distinct and they are observed as a single broadened peak. Therefore, as we increase temperature, the difference in photon energy emitted by the bright and dark state peaks effectively reduces.

In this work, we have provided an analysis of the excitonic and trionic spectra of monolayer InSe in which the negative trion has much higher binding energy and pronounced PL intensity compared to the positive trion and the exciton due to larger hole-hole interaction between these states at the VHS in the valence band. The positive trion is less bound than



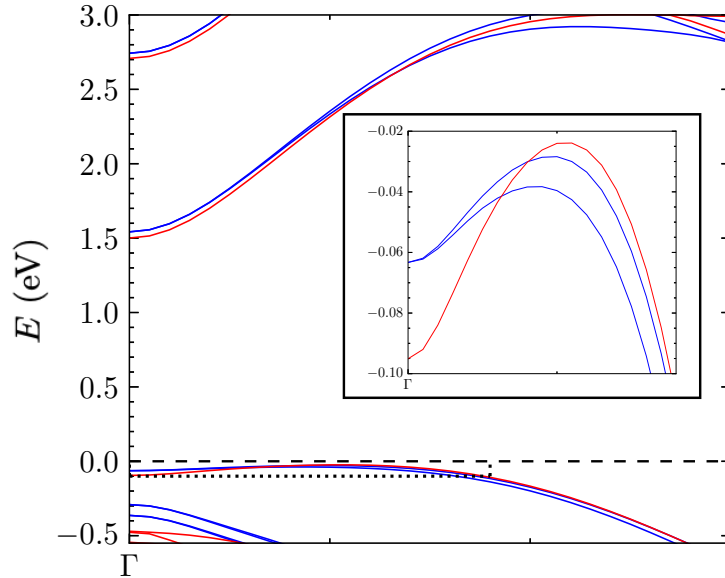


FIG. 9. Monolayer InSe band dispersion close to the  $\Gamma$ -point along the  $\Gamma - K$  direction inside the BZ, blue - with SOC, red - without SOC. Inset: Zoom in on the Mexican-hat-shaped valence band showing the different depths when SOC is included

both the exciton and the negative trion. Therefore, it is less energetically favourable in InSe.

We further show how coupling to phonons can efficiently brighten the momentum-dark states, given the small Mexican-hat depth. This effect allows us to visualise the states through photoluminescence. Although we have taken as a paradigm the widely studied system InSe, the work can be easily extended to systems with different energy depths (energy difference between  $\Gamma$ -point and VBM) of the Mexican-hat energy dispersion. For example, GaSe and InTe (and other III-VI metal chalcogenides) have been shown to also exhibit an inverted Mexican-hat in the top-most valence band [57, 58]. To examine the trend in more detail, we consider the effect of the SOC on the shape of the bands of InSe determined via DFT calculations. The inclusion of SOC lifts spin degeneracy over the BZ. However, the effects around the  $\Gamma$ -point are minimal. In the inset of Fig. 9, one can view the degeneracy lifting, which is not significant in this case. As a consequence, the binding energy is largely unaffected by the inclusion of SOC splitting and the interaction of the bands. A more notable change is that the Mexican-hat dispersion in the top-most valence band is more shallow. The effect of this is that the activation energy of the dark excitonic state is reduced. In the case of systems with a deeper Mexican-hat, the activation energy is subsequently larger,

which means that if we assume the bright state has the same binding energy, the resulting darker state will be further away in the PL spectrum. The result of this is that the dark PL peak is identifiable at higher temperatures.

In addition, this work can also account for small strain effects in monolayer InSe; this is because the strain-affected band structure of monolayer InSe is seen as a simple reduction in the bandgap due to a shifting of the conduction band energy [59], which will not affect the result of the binding energies in this model. This work further clarifies the effects of constituent particles occupying a flat band and/or systems with a VHS in the examples of the bound quasi-particle structures presented. These findings may stimulate further experimental and theoretical research on optoelectronic and semiconductor-like devices with similar energy dispersion characteristics.

## II. METHODS

### A. Exciton

To find the energy dispersion of the exciton described in monolayer InSe, we solve the Bethe-Salpeter equation (BSE) using the variational method. To describe the excitonic system comprising the conduction and valence band, we define the creation operator of the exciton, which acts on the ground-state of the system:

$$\Psi_{ex}^\dagger = \frac{1}{\sqrt{A}} \sum_{\mathbf{k}} \phi(\mathbf{k}) c_{\mathbf{k}+\mathbf{Q}}^\dagger b_{\mathbf{k}} |GS\rangle \quad (22)$$

where  $c_{\mathbf{k}+\mathbf{Q}}^\dagger$  is the creation operator of an electron in the conduction band with wave vector  $\mathbf{k} + \mathbf{Q}$ , and  $b_{\mathbf{k}}$  annihilates an electron in the valence band with wave vector  $\mathbf{k}$ , creating the corresponding hole.

The Hamiltonian of the monolayer system is given by:

$$H = H_0 + H_{int}, \quad (23)$$

where

$$H_0 = \sum_{\mathbf{k}} E_c(\mathbf{k}) c_{\mathbf{k}}^\dagger c_{\mathbf{k}} + \sum_{\mathbf{k}} E_v(\mathbf{k}) b_{\mathbf{k}}^\dagger b_{\mathbf{k}} \quad (24)$$

is the non-interacting Hamiltonian, which describes the kinetic energy of the system.

$$H_{int} = \frac{1}{2A} \sum_{\mathbf{k}_3, \mathbf{k}_4, \mathbf{q}} V(\mathbf{q}) \mathcal{F}(\mathbf{k}_3, \mathbf{k}_4, \mathbf{q}) c_{\mathbf{k}_4+\mathbf{q}}^\dagger b_{\mathbf{k}_3-\mathbf{q}}^\dagger b_{\mathbf{k}_3} c_{\mathbf{k}_4} \quad (25)$$

is the interaction Hamiltonian within which  $V(\mathbf{q})$  describes the interaction potential, and  $\mathcal{F}$  is the form factor corresponding to the overlap of the electronic states. To obtain the eigenvalue equation for the exciton, the standard procedure [60] is to first compute the bosonic commutation relation between the Hamiltonian, Eq. (23), with the exciton creation operator, Eq. (22), and then to compute the fermionic commutation relation with the same quantities. As these commutation relations are equal, this procedure provides the BSE equation [60, 61]:

$$E_{ex}\Psi_{ex}^\dagger = (E_c(\mathbf{k} + \mathbf{Q}) - E_v(\mathbf{k}))\Psi_{ex}^\dagger + \frac{1}{A} \sum_{\mathbf{k}, \mathbf{q}} \phi(\mathbf{k} - \mathbf{q})V(\mathbf{q})c_{\mathbf{k}+\mathbf{Q}}^\dagger b_{\mathbf{k}} \quad (26)$$

where  $E_{ex}$  is the exciton energy. Using Eq. (22) the above expression can be reduced to [60]:

$$E_{ex}\phi(\mathbf{k}) = [E_c(\mathbf{k}) - E_v(\mathbf{k} - \mathbf{Q})]\phi(\mathbf{k}) + \frac{1}{A} \sum_{\mathbf{q}} \phi(\mathbf{k} - \mathbf{q})V(\mathbf{q}) \quad (27)$$

The form factor,  $\mathcal{F}$ , in Eq. (25) is set to 1. In principle, the form factor is calculated using the eigenvectors of the electronic states (such as from the tight-binding model)

$$u_{\mathbf{k}_3+\mathbf{q},c}^\dagger u_{\mathbf{k}_3,c} u_{\mathbf{k}_4-\mathbf{q},v}^\dagger u_{\mathbf{k}_4,v} \quad (28)$$

where  $u_{\mathbf{k},\lambda}$  is the eigenvectors for the  $\lambda$  band. This approximation leads to the exciton description similar to a Wannier exciton [46, 60].

The interaction term,  $V(\mathbf{q})$ , used here is the Fourier transform of the Rytova-Keldysh potential

$$V(\mathbf{q}) = \frac{-2\pi e^2}{\sqrt{\kappa_z \kappa_{||}}} \frac{1}{|\mathbf{q}|(1 + r_0|\mathbf{q}|)}, \quad (29)$$

where  $r_0$  is the screening length:

$$r_0 = \frac{\sqrt{\varepsilon_z \varepsilon_{||}} - 1}{2\sqrt{\kappa_z \kappa_{||}}} d, \quad (30)$$

$\varepsilon_z, \varepsilon_{||}$  are the in and out-of-plane permittivity of InSe and  $\kappa_z, \kappa_{||}$  are the permittivities of the dielectric environment that encompasses the monolayer InSe structure. In this work, we assume the monolayer is encapsulated by hBN [46]. Thus, the parameters are [46]:  $\varepsilon_z = 9.5$ ,  $\varepsilon_{||} = 8.6$ ,  $\kappa_z = 6.9$ ,  $\kappa_{||} = 3.7$  and  $d = 8.32 \text{ \AA}$  where  $d$  represents the InSe layer thickness. To compute the excitonic ground-state through the variational method, we take as a trial wave function the hydrogenic  $1s$  state [60, 62], in an anisotropic form [18, 63]:

$$\phi_A(\mathbf{k}) = \frac{\sqrt{8\pi/\lambda} \beta^2}{(\beta^2 + k_x^2 + k_y^2/\lambda^2)^{3/2}} \quad (31)$$

Here,  $\beta$ , which is the inverse radius of the wave function and  $\lambda$ , which controls the dimensionless anisotropy, are the variational parameters to be determined. This expression is the Fourier transform of the real space wave function  $\phi_A(\mathbf{r}) \propto \exp(-\beta\sqrt{r_x^2 + (\lambda r_y)^2})$ .

We minimise the expectation value of the excitonic energy,  $E_{ex}(\mathbf{Q})$ , via the trial variational wave function  $\phi(\mathbf{k})$ . To evaluate the integral over the first Brillouin zone, we use the Monkhorst-Pack grid, [64, 65], which generates a set of  $k$ -points from the defined reciprocal lattice. We focus on a region near the  $\Gamma$ -point where the Mexican-hat is defined.

The expression for the exciton energy  $E_{ex}(\mathbf{Q})$  becomes:

$$\begin{aligned}
E_{ex}(\mathbf{Q}) & \sum_{\mathbf{k}}^{FBZ} \phi_A^*(\mathbf{k}) \phi_A(\mathbf{k}) \\
& = \min_{\beta, \lambda} \left( \sum_{\mathbf{k}}^{FBZ} \left[ \phi_A^*(\mathbf{k}) \left[ E_c(\mathbf{k}) - E_v(\mathbf{k} - \mathbf{Q}) \right] \phi_A(\mathbf{k}) + \frac{1}{AN} \sum_{\mathbf{k}'}^{FBZ} V(\mathbf{k} - \mathbf{k}') \phi(\mathbf{k}') \right] \right) \quad (32)
\end{aligned}$$

where the summation of  $\mathbf{k}'$  is over the Monkhorst-Pack grid points while keeping  $\mathbf{k} - \mathbf{k}'$  inside the BZ and contributions from  $\mathbf{k} = \mathbf{k}'$  are ignored.

## B. Trion

The extension for the ground-state trion follows the exciton, with the addition of the extra hole or electron of the opposite spin to the one previously involved with the exciton. This describes the positive and negative singlet trion systems. Their creation operators are:

$$\begin{aligned}
\Psi_{tr,+}^\dagger & = \frac{1}{\sqrt{A}} \sum_{\mathbf{k}_1, \mathbf{k}_2} \phi_{tr}(\mathbf{k}_1, \mathbf{k}_2) c_{\mathbf{k}_1 + \mathbf{k}_2 + \mathbf{Q}, \uparrow}^\dagger b_{\mathbf{k}_1, \uparrow} b_{\mathbf{k}_2, \downarrow} \\
\Psi_{tr,-}^\dagger & = \frac{1}{\sqrt{A}} \sum_{\mathbf{k}_1, \mathbf{k}_2} \phi_{tr}(\mathbf{k}_1, \mathbf{k}_2) c_{\mathbf{k}_1 + \mathbf{Q}, \uparrow}^\dagger c_{\mathbf{k}_2, \downarrow}^\dagger b_{\mathbf{k}_1 + \mathbf{k}_2, \uparrow}
\end{aligned} \quad (33)$$

Taking into account the interaction terms for the three fermions, the eigenvalue equations for the positive and negative trions are:

$$\begin{aligned}
E_{tr,+}(\mathbf{Q})\phi_{tr}(\mathbf{k}_1, \mathbf{k}_2) &= [E_c(\mathbf{k}_1 + \mathbf{k}_2) - E_{v_1}(\mathbf{k}_1 - \mathbf{Q}) - E_{v_2}(\mathbf{k}_2)] \phi_{tr}(\mathbf{k}_1, \mathbf{k}_2) \\
&+ \sum_{\mathbf{q}} V(\mathbf{q})\phi_{tr}(\mathbf{k}_1 - \mathbf{q}, \mathbf{k}_2) + \sum_{\mathbf{q}} V(\mathbf{q})\phi_{tr}(\mathbf{k}_1, \mathbf{k}_2 - \mathbf{q}) \\
&- \sum_{\mathbf{q}} V(\mathbf{q})\phi_{tr}(\mathbf{k}_1 + \mathbf{q}, \mathbf{k}_2 - \mathbf{q})
\end{aligned} \tag{34}$$

$$\begin{aligned}
E_{tr,-}(\mathbf{Q})\phi_{tr}(\mathbf{k}_1, \mathbf{k}_2) &= [E_{c_1}(\mathbf{k}_1) + E_{c_2}(\mathbf{k}_2) - E_v(\mathbf{k}_1 + \mathbf{k}_2 - \mathbf{Q})] \phi_{tr}(\mathbf{k}_1, \mathbf{k}_2) \\
&+ \sum_{\mathbf{q}} V(\mathbf{q})\phi_{tr}(\mathbf{k}_1 - \mathbf{q}, \mathbf{k}_2) + \sum_{\mathbf{q}} V(\mathbf{q})\phi_{tr}(\mathbf{k}_1, \mathbf{k}_2 - \mathbf{q}) \\
&- \sum_{\mathbf{q}} V(\mathbf{q})\phi_{tr}(\mathbf{k}_1 + \mathbf{q}, \mathbf{k}_2 - \mathbf{q})
\end{aligned}$$

where  $V(\mathbf{q})$  is the Rytova-Keldysh potential given by Eq. (29). The new variational trial function for the trion has the form [62, 66]:

$$\phi_{tr}(\mathbf{k}_1, \mathbf{k}_2) = A(\phi_{\alpha,\beta}(\mathbf{k}_1)\phi_{\gamma,\kappa}(\mathbf{k}_2) \times (-1)^S \phi_{\alpha,\beta}(\mathbf{k}_2)\phi_{\gamma,\kappa}(\mathbf{k}_1)) \tag{35}$$

It comprises the exciton states previously used (see Eq. (31)) for a respective  $\mathbf{k}$  and pair of variational parameters either  $(\alpha, \beta)$  or  $(\gamma, \kappa)$  in which each pair describes the inverse size of the respective electron-hole pair and the corresponding degree of anisotropy in the system. The factor  $(-1)^S$  determines the nature of the singlet/triplet state. We define  $\phi_{tr}(\mathbf{k}_1, \mathbf{k}_2)$  using Eq. (35) with the 1s hydrogen ground-state wave-functions:

$$\begin{aligned}
\phi_{tr}^{1s}(\mathbf{k}_1, \mathbf{k}_2) &= \left( \frac{1}{(\alpha^2 + k_{1x}^2 + k_{1y}^2/\beta^2)^{3/2}} \times \frac{1}{(\gamma^2 + k_{2x}^2 + k_{2y}^2/\kappa^2)^{3/2}} \right. \\
&\quad \left. + \frac{1}{(\alpha^2 + k_{2x}^2 + k_{2y}^2/\beta^2)^{3/2}} \times \frac{1}{(\gamma^2 + k_{1x}^2 + k_{1y}^2/\kappa^2)^{3/2}} \right)
\end{aligned} \tag{36}$$

and employ the same processes used to calculate Eq. (32) from Eq. (27), to obtain the trion energy.

### C. Phonon Coupling

To account for the brightening of the dark state described in Sec. ID, and highlighted in Fig. 4, we start by considering a polaron picture. This can be thought of as the combination

of electron-phonon and hole-phonon polarons, which make up the excitonic system. The contribution of the phonons to the electron or hole system is then given by the following term [67–69]:

$$\pm \frac{2}{A_{BZ}} \int_{BZ} d\mathbf{q}' \sum_{\nu} B_{\nu}(\mathbf{q}') g_{\nu}^*(\mathbf{k}, \mathbf{q}') A(\mathbf{k} + \mathbf{q}') \quad (37)$$

$\pm$  is the change in energy due to absorption/emission of the phonon,  $g$  represents the electron-phonon coupling,  $\nu$  is the phonon mode,  $\mathbf{q}'$  is the phonon momentum and  $A, B$  are envelope functions.  $B_{\nu}$  takes the form [69]:

$$B_{\nu}(\mathbf{q}) = \frac{g_{\nu}(\mathbf{k}, \mathbf{q}')}{\hbar\omega_{\nu}(\mathbf{q}')} \frac{1}{A_{BZ}} \int_{BZ} d\mathbf{k} A^*(\mathbf{k} + \mathbf{q}') A(\mathbf{k}) \quad (38)$$

As discussed in Sec. ID, hole-phonon scattering dominates over electron-phonon scattering. Therefore, we consider only the hole-phonon coupling, which can be represented as an eigenvalue-type expression for the change in valence band energy, which, in turn, is reduced to a simple scattering term for a single phonon. Initially, we have the following:

$$E_v(\mathbf{k}) A(\mathbf{k}) \pm \frac{2}{N} \sum_{(\mathbf{q}'), \nu} B(\mathbf{q}') g^*(\mathbf{k}, \mathbf{q}') A(\mathbf{k} + \mathbf{q}') = E_{v,ph}(\mathbf{k}) A(\mathbf{k}) \quad (39)$$

Taking the expectation value of the expression above to obtain  $E_{v,ph}$  we have:

$$\begin{aligned} \int d\mathbf{k} E_v(\mathbf{k}) A^*(\mathbf{k}) A(\mathbf{k}) \pm \frac{2}{N} \int d\mathbf{k} A^*(\mathbf{k}) \sum_{(\mathbf{q}')} B(\mathbf{q}') g^*(\mathbf{k}, \mathbf{q}') A(\mathbf{k} + \mathbf{q}') \\ = \int d\mathbf{k} E_{v,p}(\mathbf{k}) A^*(\mathbf{k}) A(\mathbf{k}) \end{aligned} \quad (40)$$

Here we can see that:

$$\frac{1}{A_{BZ}} \int d\mathbf{k} A^*(\mathbf{k}) g^*(\mathbf{k}, \mathbf{q}') A(\mathbf{k} + \mathbf{q}') = B^*(\mathbf{q}') \hbar\omega(\mathbf{q}') \quad (41)$$

Hence, the term in Eq. (37) can be rewritten as:

$$\pm \sum_{\mathbf{q}'} |B(\mathbf{q}')|^2 \hbar\omega(\mathbf{q}') \quad (42)$$

where  $|B(\mathbf{q}')|^2$  represents the average number of phonons involved in the polaron [67, 68]. As we are interested in the dominant phonon coupling, which efficiently scatters the hole at the brim of the Mexican-hat to the  $\Gamma$ -point, we consider the coupling of a single LA phonon at  $\mathbf{q}' = \mathbf{k}_{max}$  which implies that  $|B(\mathbf{q}')|^2 = 1$  for the particular value of  $\mathbf{q}'$ . As a result:

$$\sum_{\mathbf{q}'} |B(\mathbf{q}')|^2 \hbar\omega(\mathbf{q}') = \hbar\omega(\mathbf{k}_{max}) \quad (43)$$

describes the energy of the phonon,  $E_{phonon}$  and  $\mathbf{k}_{max}$ , is indicated on the phonon dispersion in Fig. 5.

We can account for this polaron system resulting from the simple hole-phonon coupling by introducing the trial wave function,  $A(\mathbf{k})$ , which takes the same form as for the exciton:

$$A(\mathbf{k}) = \frac{1}{(\beta'^2 + k_x^2 + k_y^2/\lambda^2)^{3/2}}. \quad (44)$$

here  $\beta'$  represents the inverse size of the polaron radius, and  $\lambda$  describes the anisotropy in the system. This leads to the expression for the virtual-bright state accounting for the change in the valence band term as:

$$\begin{aligned} E_{ex,ph}(\mathbf{Q}') \sum_{\mathbf{k}} A^*(\mathbf{k})A(\mathbf{k}) = & \\ & \sum_{\mathbf{k}} A^*(\mathbf{k})(E_c(\mathbf{k}) - E_v(\mathbf{k} - \mathbf{Q} - \mathbf{k}_{max}))A(\mathbf{k}) \\ & + E_{phonon} \\ & + \frac{1}{AN} \sum_{\mathbf{k}} A^*(\mathbf{k}) \sum_{\mathbf{k}'} V(\mathbf{k} - \mathbf{k}')A(\mathbf{k}') \end{aligned} \quad (45)$$

in which the valence band term,  $E_v(\mathbf{k} - \mathbf{Q} + \mathbf{k}_{max})$ , describes the momenta change due to the emission of the LA phonon.

#### D. Computational Details

In this work, the minimisation/variational technique was used in conjunction with the BlackBoxOptim.jl package in the Julia language [70]. The DFT calculations in this paper use the PBE exchange-correlation functional as implemented in Quantum Espresso [71–73] in which for the band structure calculation (with and without SOC) the cutoffs for the wavefunction and charge density are 90 Ry and 720 Ry respectively on a  $k$ -point grid of  $12 \times 12 \times 1$ , for the phonon calculation a larger  $k$ -point grid size of  $20 \times 20 \times 1$  is used with a  $q$ -point grid of  $8 \times 8 \times 1$ .

---

[1] A. C. Ferrari, F. Bonaccorso, V. Fal'Ko, K. S. Novoselov, S. Roche, P. Bøggild, S. Borini, F. H. Koppens, V. Palermo, N. Pugno, *et al.*, *Nanoscale* **7**, 4598 (2015).

- [2] P. Miró, M. Audiffred, and T. Heine, *Chemical Society Reviews* **43**, 6537 (2014).
- [3] G. R. Bhimanapati, Z. Lin, V. Meunier, Y. Jung, J. Cha, S. Das, D. Xiao, Y. Son, M. S. Strano, V. R. Cooper, *et al.*, *ACS nano* **9**, 11509 (2015).
- [4] G. Fiori, F. Bonaccorso, G. Iannaccone, T. Palacios, D. Neumaier, A. Seabaugh, S. K. Banerjee, and L. Colombo, *Nature nanotechnology* **9**, 768 (2014).
- [5] F. Koppens, T. Mueller, P. Avouris, A. Ferrari, M. S. Vitiello, and M. Polini, *Nature nanotechnology* **9**, 780 (2014).
- [6] X. Zheng and X. Zhang, in *Advances in Condensed-Matter and Materials Physics*, edited by J. Thirumalai and S. I. Pokutnyi (IntechOpen, Rijeka, 2019) Chap. 2.
- [7] X. Chen, Z. Lian, Y. Meng, L. Ma, and S.-F. Shi, *Nature Communications* **14**, 8233 (2023).
- [8] S. Borghardt, J. Sonntag, J.-S. Tu, T. Taniguchi, K. Watanabe, B. Beschoten, C. Stampfer, and B. E. Kardynał, *Opt. Mater. Express* **10**, 1273 (2020).
- [9] C. Robert, B. Han, P. Kapuscinski, A. Delhomme, C. Faugeras, T. Amand, M. R. Molas, M. Bartos, K. Watanabe, T. Taniguchi, B. Urbaszek, M. Potemski, and X. Marie, *Nature Communications* **11**, 4037 (2020).
- [10] M. Feierabend, S. Brem, A. Ekman, and E. Malic, *2D Materials* **8**, 015013 (2020).
- [11] M. Selig, G. Berghäuser, M. Richter, R. Bratschitsch, A. Knorr, and E. Malic, *2D Materials* **5**, 035017 (2018).
- [12] J. Madéo, M. K. Man, C. Sahoo, M. Campbell, V. Pareek, E. L. Wong, A. Al-Mahboob, N. S. Chan, A. Karmakar, B. M. K. Mariserla, *et al.*, *Science* **370**, 1199 (2020).
- [13] E. Malic, M. Selig, M. Feierabend, S. Brem, D. Christiansen, F. Wendler, A. Knorr, and G. Berghäuser, *Phys. Rev. Mater.* **2**, 014002 (2018).
- [14] M. Gramlich, M. W. Swift, C. Lampe, J. L. Lyons, M. Döblinger, A. L. Efros, P. C. Sercel, and A. S. Urban, *Advanced Science* **9**, 2103013 (2022).
- [15] J. Lindlau, M. Selig, A. Neumann, L. Colombier, J. Förste, V. Funk, M. Förg, J. Kim, G. Berghäuser, T. Taniguchi, K. Watanabe, F. Wang, E. Malic, and A. Högele, *Nature Communications* **9**, 2586 (2018).
- [16] Z. Li, T. Wang, C. Jin, Z. Lu, Z. Lian, Y. Meng, M. Blei, M. Gao, T. Taniguchi, K. Watanabe, *et al.*, *ACS nano* **13**, 14107 (2019).
- [17] M. Feierabend, S. Brem, A. Ekman, and E. Malic, *2D Materials* **8**, 015013 (2020).
- [18] B. Skinner, *Phys. Rev. B* **93**, 235110 (2016).



- [19] Y. Liu, A. Elbanna, W. Gao, J. Pan, Z. Shen, and J. Teng, *Advanced Materials* **34**, 2107138 (2022).
- [20] D. Huang, J. Choi, C.-K. Shih, and X. Li, *Nature Nanotechnology* **17**, 227 (2022).
- [21] H. Guo, X. Zhang, and G. Lu, *Science advances* **6**, eabc5638 (2020).
- [22] Y. You, X.-X. Zhang, T. C. Berkelbach, M. S. Hybertsen, D. R. Reichman, and T. F. Heinz, *Nature Physics* **11**, 477 (2015).
- [23] A. Esser, R. Zimmermann, and E. Runge, *physica status solidi (b)* **227**, 317 (2001).
- [24] A. Singh, G. Moody, K. Tran, M. E. Scott, V. Overbeck, G. Berghäuser, J. Schaibley, E. J. Seifert, D. Pleskot, N. M. Gabor, *et al.*, *Physical Review B* **93**, 041401 (2016).
- [25] D. Andronikov, V. Kochereshko, A. Platonov, T. Barrick, S. A. Crooker, and G. Karczewski, *Phys. Rev. B* **72**, 165339 (2005).
- [26] F. Rana, O. Koksall, and C. Manolatu, *Phys. Rev. B* **102**, 085304 (2020).
- [27] O. Koksall, M. Jung, C. Manolatu, A. N. Vamivakas, G. Shvets, and F. Rana, *Physical Review Research* **3**, 033064 (2021).
- [28] N. T. Paylaga, C.-T. Chou, C.-C. Lin, T. Taniguchi, K. Watanabe, R. Sankar, Y.-h. Chan, S.-Y. Chen, and W.-H. Wang, *npj 2D Materials and Applications* **8**, 12 (2024).
- [29] Y. Tang, K. F. Mak, and J. Shan, *Nature communications* **10**, 4047 (2019).
- [30] T. Mueller and E. Malic, *npj 2D Materials and Applications* **2**, 29 (2018).
- [31] S. Golovynskiy, O. I. Datsenko, D. Dong, Y. Lin, I. Irfan, B. Li, D. Lin, and J. Qu, *The Journal of Physical Chemistry C* **125**, 17806 (2021).
- [32] E. Liu, J. van Baren, Z. Lu, M. M. Altairy, T. Taniguchi, K. Watanabe, D. Smirnov, and C. H. Lui, *Phys. Rev. Lett.* **123**, 027401 (2019).
- [33] R. Perea-Causin, S. Brem, O. Schmidt, and E. Malic, *Physical Review Letters* **132**, 036903 (2024).
- [34] Y. Ma, Y. Dai, L. Yu, C. Niu, and B. Huang, *New Journal of Physics* **15**, 073008 (2013).
- [35] G. W. Mudd, S. A. Svatek, T. Ren, A. Patané, O. Makarovskiy, L. Eaves, P. H. Beton, Z. D. Kovalyuk, G. V. Lashkarev, Z. R. Kudrynskiy, *et al.*, *Advanced Materials (Deerfield Beach, Fla.)* **25**, 5714 (2013).
- [36] M. Yüksek, H. G. Yaglioglu, A. Elmali, E. M. Aydın, U. Kürüm, and A. Ateş, *Optics Communications* **310**, 100 (2014).

- [37] G. Mudd, M. Molas, X. Chen, V. Zólyomi, K. Nogajewski, Z. Kudrynskiy, Z. Kovalyuk, G. Yusa, O. Makarovskiy, L. Eaves, *et al.*, Scientific Reports **6**, 39619 (2016).
- [38] D. A. Bandurin, A. V. Tyurnina, G. L. Yu, A. Mishchenko, V. Zólyomi, S. V. Morozov, R. K. Kumar, R. V. Gorbachev, Z. R. Kudrynskiy, S. Pezzini, *et al.*, Nature nanotechnology **12**, 223 (2017).
- [39] T. Shubina, W. Desrat, M. Moret, A. Tiberj, O. Briot, V. Y. Davydov, A. Platonov, M. Semina, and B. Gil, Nature communications **10**, 3479 (2019).
- [40] S. Slizovskiy, A. V. Chubukov, and J. J. Betouras, Physical review letters **114**, 066403 (2015).
- [41] S. Slizovskiy, J. J. Betouras, S. T. Carr, and J. Quintanilla, Physical Review B **90**, 165110 (2014).
- [42] L. Classen and J. J. Betouras, arXiv preprint arXiv:2405.20226 (2024).
- [43] A. Chandrasekaran, L. C. Rhodes, E. A. Morales, C. A. Marques, P. D. C. King, P. Wahl, and J. J. Betouras, Nature Communications **15**, 9521 (2024).
- [44] A. Chandrasekaran and J. J. Betouras, Advanced Physics Research **2**, 2200061 (2023).
- [45] J. Zultak, S. J. Magorrian, M. Koperski, A. Garner, M. J. Hamer, E. Tóvári, K. S. Novoselov, A. A. Zhukov, Y. Zou, N. R. Wilson, *et al.*, Nature Communications **11**, 125 (2020).
- [46] A. Ceferino, K. W. Song, S. J. Magorrian, V. Zólyomi, and V. I. Fal’ko, Phys. Rev. B **101**, 245432 (2020).
- [47] S. J. Magorrian, V. Zólyomi, and V. I. Fal’ko, Phys. Rev. B **94**, 245431 (2016).
- [48] E. Liu, J. van Baren, Z. Lu, M. M. Altairy, T. Taniguchi, K. Watanabe, D. Smirnov, and C. H. Lui, Phys. Rev. Lett. **123**, 027401 (2019).
- [49] E. Liu, J. van Baren, Z. Lu, M. M. Altairy, T. Taniguchi, K. Watanabe, D. Smirnov, and C. H. Lui, Physical review letters **123**, 027401 (2019).
- [50] H. Wang, C. Zhang, W. Chan, C. Manolatou, S. Tiwari, and F. Rana, Phys. Rev. B **93**, 045407 (2016).
- [51] T. C. Berkelbach, M. S. Hybertsen, and D. R. Reichman, Phys. Rev. B **88**, 045318 (2013).
- [52] W. Li, S. Poncé, and F. Giustino, Nano Letters **19**, 1774 (2019).
- [53] S. Brem, A. Ekman, D. Christiansen, F. Katsch, M. Selig, C. Robert, X. Marie, B. Urbaszek, A. Knorr, and E. Malic, Nano letters **20**, 2849 (2020).
- [54] M. Feierabend, S. Brem, A. Ekman, and E. Malic, 2D Materials **8**, 015013 (2020).
- [55] J. W. Christopher, B. B. Goldberg, and A. K. Swan, Scientific reports **7**, 14062 (2017).

- [56] R. Perea-Causin, S. Brem, F. Buchner, Y. Lu, K. Watanabe, T. Taniguchi, J. M. Lupton, K.-Q. Lin, and E. Malic, *Nature Communications* **15**, 6713 (2024).
- [57] V. Zólyomi, N. Drummond, and V. Fal'Ko, *Physical Review B* **89**, 205416 (2014).
- [58] H. Cai, Y. Gu, Y.-C. Lin, Y. Yu, D. B. Geohegan, and K. Xiao, *Applied Physics Reviews* **6** (2019).
- [59] Q. Wang, L. Han, L. Wu, T. Zhang, S. Li, and P. Lu, *Nanoscale research letters* **14**, 1 (2019).
- [60] M. F. C. M. Quintela, J. C. G. Henriques, L. G. M. Tenório, and N. M. R. Peres, *physica status solidi (b)* **259**, 10.1002/pssb.202200097 (2022).
- [61] R. Tempelaar and T. C. Berkelbach, *Nature Communications* **10**, 10.1038/s41467-019-11497-y (2019).
- [62] C. Zhang, H. Wang, W. Chan, C. Manolatou, and F. Rana, *Phys. Rev. B* **89**, 205436 (2014).
- [63] E. Prada, J. V. Alvarez, K. L. Narasimha-Acharya, F. J. Bailen, and J. J. Palacios, *Phys. Rev. B* **91**, 245421 (2015).
- [64] H. J. Monkhorst and J. D. Pack, *Phys. Rev. B* **13**, 5188 (1976).
- [65] J. D. Pack and H. J. Monkhorst, *Phys. Rev. B* **16**, 1748 (1977).
- [66] Y.-W. Chang and Y.-C. Chang, *The Journal of Chemical Physics* **155**, 10.1063/5.0057493 (2021).
- [67] W. H. Sio, C. Verdi, S. Poncé, and F. Giustino, *Phys. Rev. Lett.* **122**, 246403 (2019).
- [68] W. H. Sio, C. Verdi, S. Poncé, and F. Giustino, *Phys. Rev. B* **99**, 235139 (2019).
- [69] W. H. Sio and F. Giustino, *Nature Physics* **19**, 629–636 (2023).
- [70] R. Feldt, P. Nordin, R. Thorngren, and E. Cronholm, *Blackboxoptim.jl: A global optimization package for julia* (2023), version 0.6.3.
- [71] P. Giannozzi, S. Baroni, N. Bonini, M. Calandra, R. Car, C. Cavazzoni, D. Ceresoli, G. L. Chiarotti, M. Cococcioni, I. Dabo, A. Dal Corso, S. de Gironcoli, S. Fabris, G. Fratesi, R. Gebauer, U. Gerstmann, C. Gougoussis, A. Kokalj, M. Lazzeri, L. Martin-Samos, N. Marzari, F. Mauri, R. Mazzarello, S. Paolini, A. Pasquarello, L. Paulatto, C. Sbraccia, S. Scandolo, G. Sclauzero, A. P. Seitsonen, A. Smogunov, P. Umari, and R. M. Wentzcovitch, *Journal of Physics: Condensed Matter* **21**, 395502 (19pp) (2009).
- [72] P. Giannozzi, O. Andreussi, T. Brumme, O. Bunau, M. B. Nardelli, M. Calandra, R. Car, C. Cavazzoni, D. Ceresoli, and e. a. M Cococcioni, *Journal of Physics: Condensed Matter* **29**, 465901 (2017).

- [73] P. Giannozzi, O. Baseggio, P. Bonfà, D. Brunato, R. Car, I. Carnimeo, C. Cavazzoni, S. de Gironcoli, P. Delugas, F. Ferrari Ruffino, A. Ferretti, N. Marzari, I. Timrov, A. Urru, and S. Baroni, *The Journal of Chemical Physics* **152**, 154105 (2020).

### **III. ACKNOWLEDGEMENTS**

We thank Nicholas Hine and Samuel Magorrian for useful discussions. We are grateful to the UK Engineering and Physical Sciences Research Council for funding via Grant No EP/T034351/1.

### **IV. AUTHOR CONTRIBUTIONS**

LJB performed the calculations, MTG and JJB initiated and supervised the project. All authors discussed the results and wrote the paper.

### **V. COMPETING INTERESTS**

The authors declare no competing interests.